

Research Article

Open Access



Electro-assisted assembly of conductive polymer and soft hydrogel into core-shell hybrids

Aruã Clayton Da Silva^{1,2,*}, Thomas Edward Paterson¹, Ivan Rusev Minev^{1,2,3,*}

¹Department of Automatic Control and Systems Engineering, Faculty of Engineering, University of Sheffield, Sheffield S1 3JD, UK.

²Insigneo Institute for in silico Medicine, University of Sheffield, Sheffield S1 3JD, UK.

³Leibniz Institute of Polymer Research Dresden, Dresden 01069, Germany.

***Correspondence to:** Dr. Aruã Clayton Da Silva, Department of Automatic Control and Systems Engineering, Faculty of Engineering, University of Sheffield, Sheffield S1 3JD, UK. E-mail: a.dasilva@sheffield.ac.uk; Prof. Ivan Rusev Minev, Department of Automatic Control and Systems Engineering, Faculty of Engineering, University of Sheffield, Sheffield S1 3JD, UK. E-mail: i.minev@sheffield.ac.uk

How to cite this article: Da Silva AC, Paterson TE, Minev IR. Electro-assisted assembly of conductive polymer and soft hydrogel into core-shell hybrids. *Soft Sci* 2023;3:3. <https://dx.doi.org/10.20517/ss.2022.25>

Received: 28 Oct 2022 **First Decision:** 1 Dec 2022 **Revised:** 19 Dec 2022 **Accepted:** 5 Jan 2023 **Published:** 17 Jan 2023

Academic Editor: Zhifeng Ren **Copy Editor:** Fangling Lan **Production Editor:** Fangling Lan

Abstract

Soft hydrogels have become an important class of materials for mimicking and interfacing biological soft tissues with potential applications in drug delivery, tissue engineering and bioelectronics. Creative methods for integrating hydrogels with other materials such as organic conductors are highly desired. Here, we describe the single-step electrosynthesis of PEDOT/alginate into core-shell hybrid structures via an electrochemical-chemical-chemical mechanism. Using a pulsed electropolymerisation protocol, we generated PEDOT in either oxidized or reduced form. By-products of this electrochemical step trigger the chemical reactions for the concomitant assembly of alginate hydrogels. Characterization evidences that PEDOT (core) and alginate (shell) compartments form an electrochemically integrated interface. During growth, both can be loaded with useful cargo. We loaded a negatively charged small molecule and investigated passive and electroactive release mechanisms from the two compartments. Our electro-assisted assembly/crosslinking of integrated PEDOT/alginate hybrids contributes a promising approach to the design of functional interfaces for applications in controlled release and soft electronics.

Keywords: Conducting polymer, soft hydrogel, bioelectronics, hybrid materials



© The Author(s) 2023. **Open Access** This article is licensed under a Creative Commons Attribution 4.0 International License (<https://creativecommons.org/licenses/by/4.0/>), which permits unrestricted use, sharing, adaptation, distribution and reproduction in any medium or format, for any purpose, even commercially, as long as you give appropriate credit to the original author(s) and the source, provide a link to the Creative Commons license, and indicate if changes were made.



INTRODUCTION

Hydrogels are crosslinked polymer networks swollen with water (typically > 95%wt). They can be built from a wide range of natural and synthetic macromolecules. As bioengineering materials, they offer useful properties such as tissue-like viscoelasticity, tuneable degradation, three-dimensional matrix for supporting cell growth and sequestration or release of biomolecules, among others^[1,2]. A notable example is alginate (extracted from brown algae) which consists of the anionic polysaccharide alginic acid that can be crosslinked by metal ions such as Ca^{2+} . The resultant network readily absorbs water and swells to form a hydrogel with a pore size of a few nanometers^[3]. Alginate hydrogels are used in clinical devices such as wound dressings and implant coatings, as drug delivery microparticles or as cell encapsulates in bioprinting technologies^[4,5].

Hydrogels can be composed of more than one polymer network to enable hybrid functionalities. For example, the incorporation of an interpenetrating conductive polymer network results in hydrogels with mixed mode (electronic-ionic) conductivity^[6]. This is desirable for bioelectronic interfacing technologies where the hydrogel can enhance the charge injection capacity of electrodes, serve as a mechanical buffer between rigid substrates and tissue, improve cell adhesion, or facilitate drug release^[7-10]. A notable example is poly (3,4-ethylenedioxythiophene) (PEDOT) which has good electroactivity and processability when combined with a polyanion dopant^[10-16]. Although PEDOT is mostly processed in thin-film coatings, recent studies have integrated it into conductive hydrogels^[17-22]. For instance, PEDOT and alginate are often reported as composites or blends attempting to merge their constituent properties in the resulting material^[23-28].

Hydrogels can be formed by various mechanisms, including ionic or covalent crosslinks, as well as interpenetrating polymer networks^[29]. Although the electrostatic interaction is stronger and more stable in nature (e.g., minerals, rocks), due to the high water content in hydrogels, the resulting ionic crosslinks generate typically brittle materials with poor mechanical stability, as is the case with most alginate based hydrogels^[30]. This makes integration with other materials (where soft-rigid interfaces are present) challenging and may limit some practical applications^[31]. This is even more pressing in the case of conductive hydrogels, where the interface with an organic semiconductor or a metallic conductor additionally requires efficient charge exchange^[32,33]. Thus, despite remarkable progress where conductive hydrogels have achieved extreme stretchability, softness and conductivity, relatively little has been done to engineer good interfaces to other materials as will be needed in practical systems.

One option is to utilise surface functionalisation or treatments (e.g., silanization) that improve adhesion via covalent and/or ionic bonds^[31,33,34]. These methods are effective; however, they require additional steps and add complexity to the processing of hybrid structures. As an alternative, electrodeposition methods can offer a simple strategy to facilitate the direct growth of soft materials, especially over conductive substrates, controlling electron transfer and adhesion process at the interface^[32,35-38]. A number of promising electrochemical approaches have already been reported. For instance, water hydrolysis or redox mediators have been used to promote the electrogelation of a range of ionically crosslinked biomatrixes^[39-44]. Copper ions electrochemically released from a sacrificial layer have been shown to coordinate PEDOT:PSS microparticles and the formation of conductive hydrogels^[32]. Recently, we have proposed an electro-assisted method for forming hydrogels on conductive surfaces using an electrochemical-chemical-chemical (ECC) mechanism. This includes deposition of conductive hybrid PEDOT/alginate films^[36]. However, application of traditional electrodeposition protocols highlighted several limitations, such as slow growth kinetics and low levels of hydration of the final material.

In the present work, we propose an electro-assisted assembly of core-shell structures formed from PEDOT (core) and alginate hydrogel (shell). This is achieved via pulsed electrochemical protocols and the ECC mechanism, which results in significant improvement of growth kinetics of the core and shell compartments. We find that PEDOT and the alginate hydrogel form a well integrated electrochemical and mechanical interface. We explore the core-shell structures as passive/sensing release and electrically controlled delivery vehicles. In our system, the hydrogel is formed on a robust conductive substrate which improves the overall integration. This is in contrast with freestanding structures that may be difficult to handle. The strength of our approach is that even such brittle and delicate hydrogels (such as alginate) can be integrated into a device. In terms of clinical application, we envisage the hydrogels as functional coatings on electrodes that can transform a traditional electrode into a depot for drug or cell delivery.

METHODS

Materials. The chemical reagents 3,4-ethylenedioxythiophene (EDOT), sodium alginate, calcium carbonate, sodium dodecyl sulphate (SDS), fluorescein and sodium citrate were purchased from Sigma-Aldrich. All solutions were prepared with deionized Milli-Q water (18.2 M Ω) or with phosphate saline buffer (PBS) pH 7.4 (Gibco™).

Electrodeposition solution. The solution composition was adapted from a previous work^[36]. Firstly, 1.0 (w/w) of calcium carbonate was dispersed in 24.3 mL of deionized water, followed by dissolution of 1% (w/w) sodium alginate kept under vigorous stirring for 30 min at room temperature. Later, 70 mM of SDS and 50 mM of EDOT were added. As soon as the EDOT was added, the solution was placed in an electrochemical cell for further electrodeposition experiments. The key to obtaining homogeneous hydrogels was the maintenance of a uniform suspension of calcium carbonate microparticles in the electrolyte, which was ensured by constantly stirring the reaction solution (200 rpm in all experiments, [Supplementary Table 1](#)). For the model drug experiments, 1 mg mL⁻¹ of fluorescein was added before the SDS and EDOT.

Electrochemical measurements. Cyclic voltammetry (CV), chronoamperometry (CA) and electrochemical impedance spectroscopy (EIS) were performed using a potentiostat/galvanostat (PARSTAT3000, AMETEK) controlled using VersaStudio 2.60.2 software. Pulsed protocol methods were programmed a “Loop” (number of desired pulses) containing CA at electrodeposition potential (+1.4 V) for 0.5 s plus either OCP (for OCPI protocol) or CA at 0 V (for RPI protocol) for 10 s. CV traces were recorded in PBS as supporting electrolytes from -1.2 V to +0.8 V at a scan rate of 100 or 50 mV s⁻¹. EIS data were recorded from 1 MHz to 0.1 Hz, with an excitation amplitude of 10 mV (RMS) at 10 points per decade. The working electrode employed was gold wire with submersed lengths ranging from 1.27 to 2.54 cm. A commercially available Ag/AgCl/KCl 3M (BASi) electrode and a platinum coil were used as reference and counter electrodes, respectively. For statistical analysis, all experiments were made in triplicate using three different gold wire electrodes and freshly prepared solutions. Unless stated otherwise, data is reported as the mean \pm standard deviation.

All charges were calculated by $Q = I \times t$, where I is the current density (A mm⁻²) and t is time (seconds). Parameter fitting and circuit simulation were conducted using the NOVA 2.1 software (Metrohm Autolab). Resistance was calculated from the constant phase element (CPE) using the following equation^[45,46]:

$$R = \frac{1}{Y_0 (\omega''_{max})^n} \quad (1)$$

where R is resistance, Y_0 is the pseudocapacitance constant value, ω''_{max} is the frequency where the imaginary part is highest and n is the deviation from ideal capacitor ($n = 0$ is a pure resistor, $n = 1$ is a pure capacitor).

Fluorescence quantification. To quantify the concentration of the fluorescein molecule, a fluorescence spectrometer was used to measure light intensity. A reference curve was prepared using serial dilutions from 1 mg mL^{-1} to $1.5 \cdot 10^{-5} \text{ mg mL}^{-1}$. Molecule excitation was at 485 nm and emission was measured at 528 nm. The concentration of fluorescein was calculated using the reference curve using GraphPad.

Scanning electron microscopy - energy dispersive x-ray spectroscopy (SEM-EDS). A Philips/FEI XL-20 SEM (Philips, UK) scanning electron microscope was used to image dehydrated hydrogel samples. Cross section was obtained by cutting the hydrogels using a razor blade when freshly prepared. The samples were dehydrated by replacing water with ethanol and were processed in a critical point dryer (CPD). Samples were sputter coated with gold before SEM imaging. The gold-coated hydrogels were then imaged with an accelerating voltage of 15 kV.

RESULTS

Conductive Hybrid PEDOT/alginate Hydrogels. We investigated a number of electrochemical strategies to generate PEDOT/alginate hybrid hydrogels. Firstly, we attempted to use water hydrolysis (+1.85 to +2.0 V) to promote gelation of alginate in parallel with electropolymerisation of PEDOT, which also occurs in this potential window. This did not produce a core-shell structure but a hybrid hydrogel with blue colour and gel aspect [Supplementary Figure 1]. The resultant structure has poor electroactivity, likely because gas produced during water hydrolysis is removing PEDOT from the gold surface, and hence the hybrid hydrogel is electrically not well-connected to the substrate (no electroactivity). We then turned to an alternative strategy where the protons generated during EDOT polymerisation are used to promote the gelation of alginate. We added the surfactant SDS (70 mM) to the aqueous polymerisation solution to increase the concentration of EDOT monomers to $50 \text{ mM}^{[47]}$ which is expected to dramatically increase the availability of protons. This resulted in the growth of a core-shell structure with a significant amount of alginate hydrogel layer (shell) which enveloped a film of PEDOT (core) with fractal morphology [Figure 1]. Here SDS (an anionic surfactant) is chosen over other surfactants because it is compatible with the negative charges on the alginate molecule. As illustrated in Supplementary Figure 2, SDS does not precipitate the alginate solution, which means that the surfactant itself does not interfere with the electrically assisted gelation processes.

The reaction follows an electrochemical-chemical-chemical mechanism (ECC). At +1.4 V (*vs.* Ag/AgCl/KCl 3M), the EDOT monomer is electrodeposited over the gold electrode. The EDOT monomers are delivered by the SDS micelles in “patches”. This patch electrodeposition (step 1) generates protons to trigger the decomposition reaction (step 2) of calcium carbonate. The calcium carbonate acts as a buffer and stabilizes the solution pH at 9.40. The release of calcium ions in the presence of alginate macromolecules promotes the coordination (step 3), obtaining the ionically crosslinked alginate hydrogel layer [Figure 1A]. Changing the concentration of CaCO_3 in the range of 0.5%-1.5% (m/m) did not significantly affect the spatial extent of the alginate layers. This suggests that any excess Ca^{2+} contributes to strengthening existing crosslinks rather than coordinating new alginate molecules [Supplementary Figure 3]. In support of this, we observe that gels produced in electrolytes with higher CaCO_3 have the same spatial extent but tend to be stable for longer in PBS (without Ca^{2+} supplement). The alginate component disassembles uniformly (along the wire), indicating uniform composition in the radial direction [Supplementary Figure 3]. Additionally, this reaction generates carbon dioxide and water, ideal by-products according to the green chemistry principle^[48]. Figure 1B illustrates the 3-electrodes electrochemical setup. Here, we define the core-shell

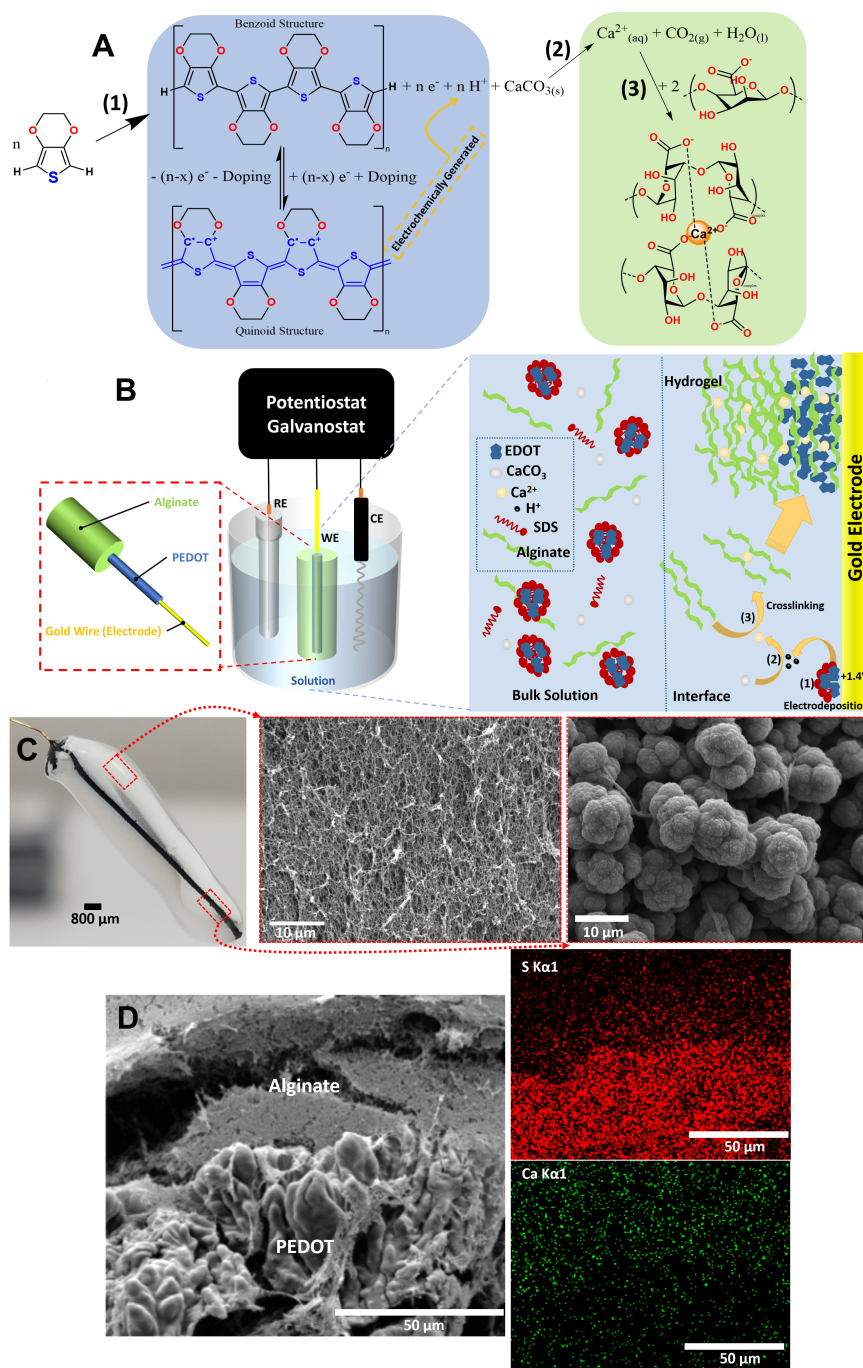


Figure 1. Electrodeposition of core-shell structures. (A) Chemical reactions involved in electropolymerisation (1) of EDOT to neutral state of PEDOT (benzoid structure, top) and redox equilibrium (blue block) to oxidized PEDOT (quinoid structure, bipolaron represented in blue, bottom) followed by (2) decomposition of calcium carbonate; and (3) complexation with alginate macromolecules representing the alginate hydrogel formation (green block). (B) Schematic representation of the 3-electrode electrochemical cell with reference electrode (RE), working electrode (WE) and counter electrode (CE). On the left, coaxial representation (red dashed square) of the core-shell structures deposited over gold wire. On the right, schematic representation (blue) of molecules and ionic species present in the bulk electrolyte, above the critical micellar concentration (CMC) and WE potential of +1.4 V (vs. Ag/AgCl/KCl 3M). The respective order of chemical reactions (1-3) leading to core-shell formation is indicated. (C) Photograph of the PEDOT/alginate structures electrodeposited over a gold wire, followed by SEM images of the alginate shell surface (middle) and PEDOT core layer (right). (D) SEM image (left) of a cross section at the PEDOT/alginate interface and atomic distribution (right) of sulphur (S, $\text{K}\alpha_1$ in red) and calcium (Ca, $\text{K}\alpha_1$ in green).

structure as having a solid core and a soft shell. On the right side, the schematic representation of “patch” electrodeposition of PEDOT is illustrated. The use of electrochemical reaction as the first step enables us to have good kinetic control over the subsequent gelation process. **Figure 1C** shows a photograph of the structures produced. The SEM image of alginate shell layer evidences the porous structure of the alginate hydrogel. The SEM image of the PEDOT core layer evidences its globular morphology, likely due to “patch” electrodeposition caused by the merging of SDS micelles. **Figure 1D** shows a cross section SEM image of the PEDOT/alginate interface with EDS (Energy Dispersive Spectrometry) mapping for sulphur and calcium elements. As expected, the PEDOT core is sulphur-rich, while the alginate hydrogel shell is crosslinked by calcium ions. Therefore, the atomic distribution clearly distinguishes the core and shell components. The presence of calcium signals in PEDOT suggests that alginate is incorporated within and likely dopes the PEDOT core. The brittle nature of the alginate hydrogel prevents us from mechanically studying the adhesion strength between the core and shell layers. However, during experiments, we did not observe delamination even when the structure was sliced for imaging [**Figure 1D**]. This indicates the absence of large residual stresses built at the interface during assembly.

Growth Kinetics of Core-Shell Hydrogels. A typical electrodeposition method is the step potential, as illustrated in **Figure 2A(i)** (constant electric potential applied for a pre-set time). Under this condition, the electropolymerisation current rapidly drops when the initial monomer concentration is depleted at the electrode’s interface. Later, it reaches an equilibrium with new monomers diffusing from the bulk solution [**Supplementary Figure 4**]. Usually, this is not an issue for simple electrodeposition processes since increasing the time increases the amount of PEDOT and subsequently the electroactivity of the deposited film [**Supplementary Figure 5**]. However, in the ECC mechanism, there are chemical steps coupled to the electrodeposition. Thus, the diffusion limitation in the first step significantly limits the chemical species available for the subsequent gelation process. In our system, this leads to the production of only a thin layer of alginate when the step potential method is applied. In order to overcome this limitation, we explored pulsed protocols where the time between pulses allows more EDOT monomers to diffuse to the reacting surface [**Supplementary Figure 6**]. Electrodeposition protocols presented in **Figure 2A(ii and iii)** consist of an electropolymerisation pulse (500 ms, +1.4 V vs. Ag/AgCl) followed by an interpulse holding potential which is either the open circuit potential (OCP) or 0 V. The polymerisation process may consist of many repetitions of the pulse-hold sequence. The pulsed protocol using OCP as hold potential will be referred to as Open Circuit Potential Interpulse (OCPI) protocol, while using 0 V as holding potential will be referred to as Reducing Potential Interpulse (RPI) protocol.

We next define the following charges: the Q_{ox}^{total} and Q_{red}^{total} as the total charges applied in each pulse for oxidation and reduction processes, respectively. $Q_{electropolymerization}$ is the charge that directly contributes to polymerisation by linking EDOT monomers, forming benzoid structure [**Figure 1A**]. $Q_{ox PEDOT}$ is the charge used to oxidize PEDOT chains (obtaining quinoid structure, **Figure 1A**) after the polymer is already formed. We assume that the charge delivered at positive electrode potentials, Q_{ox}^{total} contributes to both $Q_{electropolymerization}$ and $Q_{ox PEDOT}$. Similarly, $Q_{red PEDOT}$ is the charge expended to reduce the PEDOT from quinoid to benzoid structure. Since already formed PEDOT cannot depolymerize, charges flowing during the interpulse can only contribute to Q_{red}^{total} , thus $Q_{ox}^{total} = Q_{red PEDOT}$. Finally, Q is the summation of all charges at the end of a pulse or sequence of pulses [**Figure 2B**]; we can thus write:

$$Q = Q_{ox}^{total} + Q_{red}^{total} = Q_{electropolymerization} + Q_{ox PEDOT} + Q_{red PEDOT} \quad (2)$$

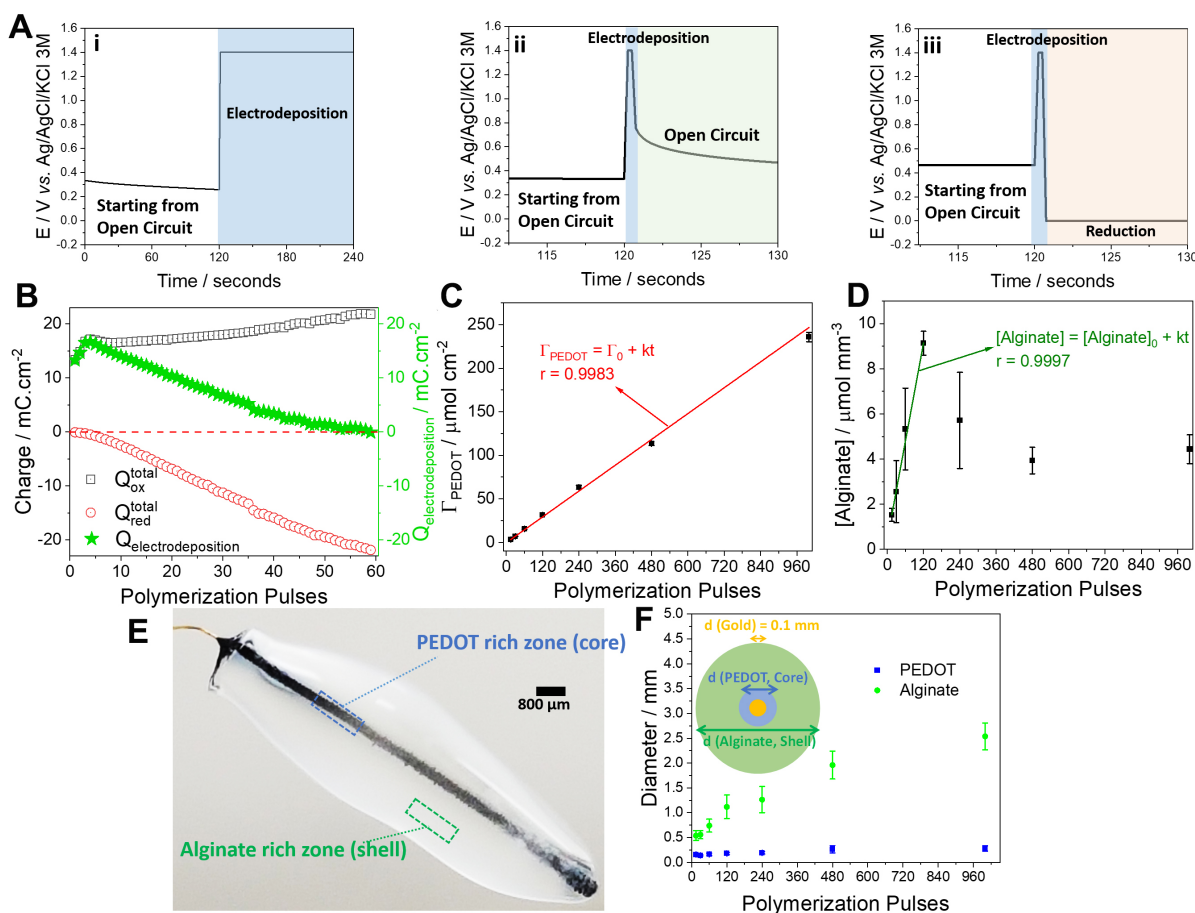


Figure 2. Growth kinetics of PEDOT/alginate structures. (A) Program for electrodeposition in (i) traditional step electric potential (electrodeposition in blue), (ii) pulses of 0.5 s (blue) followed by holding at OCP (green) for 10 s, called open circuit potential interpulse (OCPI) protocol and (iii) pulses of 0.5 s (blue) followed by holding at 0 V (reduction potential, orange), called reducing potential interpulse (RPI) protocol. (B) Charge versus number of polymerisation pulses, discriminating the total oxidation charge ($Q_{\text{ox}}^{\text{total}}$, black), the total reduction charge ($Q_{\text{red}}^{\text{total}}$, red) and the calculated actual electrodepositon charge ($Q_{\text{electrodeposition}}$, green) for the RPI protocol. (C) Kinetics of the PEDOT growth (produced using the OCPI protocol) showing zero order growth from 15 to 1000 polymerisation pulses. (D) Kinetics of the alginate hydrogel growth (produced using the OCPI protocol) showing zero order growth from 15 to 120 polymerisation pulses. (E) Photograph of the PEDOT/alginate hydrogel electrodeposited over a gold wire (13 mm length) evidencing the PEDOT (core) and alginate (shell) rich zones. (F) Growth profiles of PEDOT and alginate vs. pulse number using the OCPI protocol. Inset: Cross section scheme of the formed structure indicating the gold wire (diameter 0.1 mm), PEDOT and alginate diameters used to calculate the respective volumes.

For RPI, after a time (here empirically determined to be 60 pulses), a state where $Q_{\text{ox PEDOT}} = -Q_{\text{red PEDOT}}$ is reached. This is because, during the reducing interpulse period (electrode potential = 0 V), the current quickly drops to zero, suggesting PEDOT is left in a neutral state [Supplementary Figures 7 and 8]. This allows us to obtain $Q_{\text{electropolymerization}}$. For the OCPI protocol, we electrodeposited the hybrid hydrogel first with a pulse train and afterwards applied a long reducing pulse (0 V for 20 min) to obtain the condition where $Q_{\text{red PEDOT}} = -Q_{\text{ox PEDOT}}$. This is in contrast with step potential methods where it is not possible to directly discriminate the electrodepositon charge from the oxidation charge.

The estimate for $Q_{\text{electropolymerization}}$ therefore, allows us to determine the effective surface coverage (Γ) which quantifies the amount of polymer deposited per unit area of electrode^[49].

$$\Gamma = \frac{Q_{\text{electropolymerisation}}}{n F A} \quad (3)$$

where F is the Faraday constant ($96,486 \text{ C mol}^{-1}$), n is the number of electrons transferred in the electrodeposition process ($n = 1$, for linking two EDOT monomers) and A is the geometric area of the electrode (gold wire). Knowing $Q_{\text{electropolymerisation}}$, we also estimated the number of generated protons (reaction in [Figure 1](#)) and therefore the number of moles of Ca^{2+} released. Assuming that one Ca^{2+} is sufficient to coordinate the crosslinking of two alginate molecules, we can link the (electron) charge to the amount of alginate hydrogel produced in the shell. From the reactions described in [Figure 1](#), we can write the following stoichiometric relationship of electron:proton:calcium:alginate as $1:1:\frac{1}{2}:1$ respectively. This allowed us to obtain the kinetics of growth for both PEDOT and alginate components obtained via the OCPI protocol. As illustrated in [Figure 2C](#), the growth of the PEDOT core follows order zero with $0.25 \pm 0.01 \mu\text{mol cm}^{-2} \text{ pulse}^{-1}$ ($r = 0.9983$) for all polymerisation pulses applied. [Figure 2D](#) shows that the growth of the alginate shell follows order zero as $0.07 \pm 0.01 \mu\text{mol mm}^{-3} \text{ pulse}^{-1}$ ($r = 0.9997$) until 120 polymerisation pulses. After 120 pulses, the zero order growth kinetics breaks down. [Figure 2E](#) shows a picture of the PEDOT/alginate structure obtained with 240 pulses (OCPI), highlighting the interface of PEDOT (core, blue) and alginate (shell, green) rich zones. [Figure 2F](#) evidences the growth profile of the core and shell based on diameter increase. The diameters increase with a similar trend as discussed above using kinetics parameters [[Figure 2D](#)]. The growth profile of the alginate hydrogel presented here is similar to pure alginate formed over electrodes, tending to reach a plateau for long electrodeposition periods^[36].

Electrochemical properties of the PEDOT-Alginate interface. To investigate if the core and shell layers are electrochemically linked, we performed cyclic voltammetry and impedance spectroscopy measurements. [Figure 3A](#) shows normalized cyclic voltammograms of bare gold wire (black), PEDOT:SDS (without alginate, grey) and the PEDOT/alginate structures electrodeposited with step potential (1000 s, red), RPI (60 pulses, green) and OCPI protocols (120 pulses, blue). To enable a direct comparison, the current was normalised by the electrode area and $Q_{\text{electropolymerisation}}$. All electrochemical characterizations were made in PBS ($\text{pH} = 7.4$) as supporting electrolyte in order to simulate physiological conditions. The core-shell structure obtained using the OCPI protocol is the most electroactive. That obtained with the RPI protocol presents pseudofaradaic peaks shifted to negative potentials (starting at -0.3 V for the oxidation process). This is likely because PEDOT here is obtained in dedoped (reduced) state, so in the first cycle, it becomes doped with phosphate ions from the supporting electrolyte (PBS). All other polymerisation conditions formed the PEDOT component in its doped state (here doped with SDS/alginate) with pseudofaradaic peak starting at $+0.3 \text{ V}$. For the structures obtained with the OCPI protocol, we observe dedoping of SDS/alginate and redoping with phosphate with a pseudofaradaic process appearing around -0.3 V with an increasing number of cycles [[Supplementary Figure 9](#)]. The interface consisting of PEDOT:SDS only (without alginate) showed the lowest electroactivity. This suggests alginate as an anionic polyelectrolyte is the main dopant and is incorporated in the PEDOT core. The alginate shell layer improves the electroactivity of the entire hybrid structure. We hypothesize that the alginate layer stabilizes fractal PEDOT structures at the interface, preventing them from exfoliating and losing interconnectivity with the bulk of the PEDOT core. Among the core-shell structures, those produced via the OCPI protocol demonstrated enhanced electroactivity.

Electrochemical impedance spectroscopy (EIS) for the various deposition protocols is shown in [Figure 3B](#). Again, the structures electrodeposited using the two pulsed methods presented lower impedance when compared to PEDOT:SDS and PEDOT/alginate (step). Between the structures obtained via pulsed methods, the OCPI protocol shows a reduced total impedance, especially for lower frequencies.

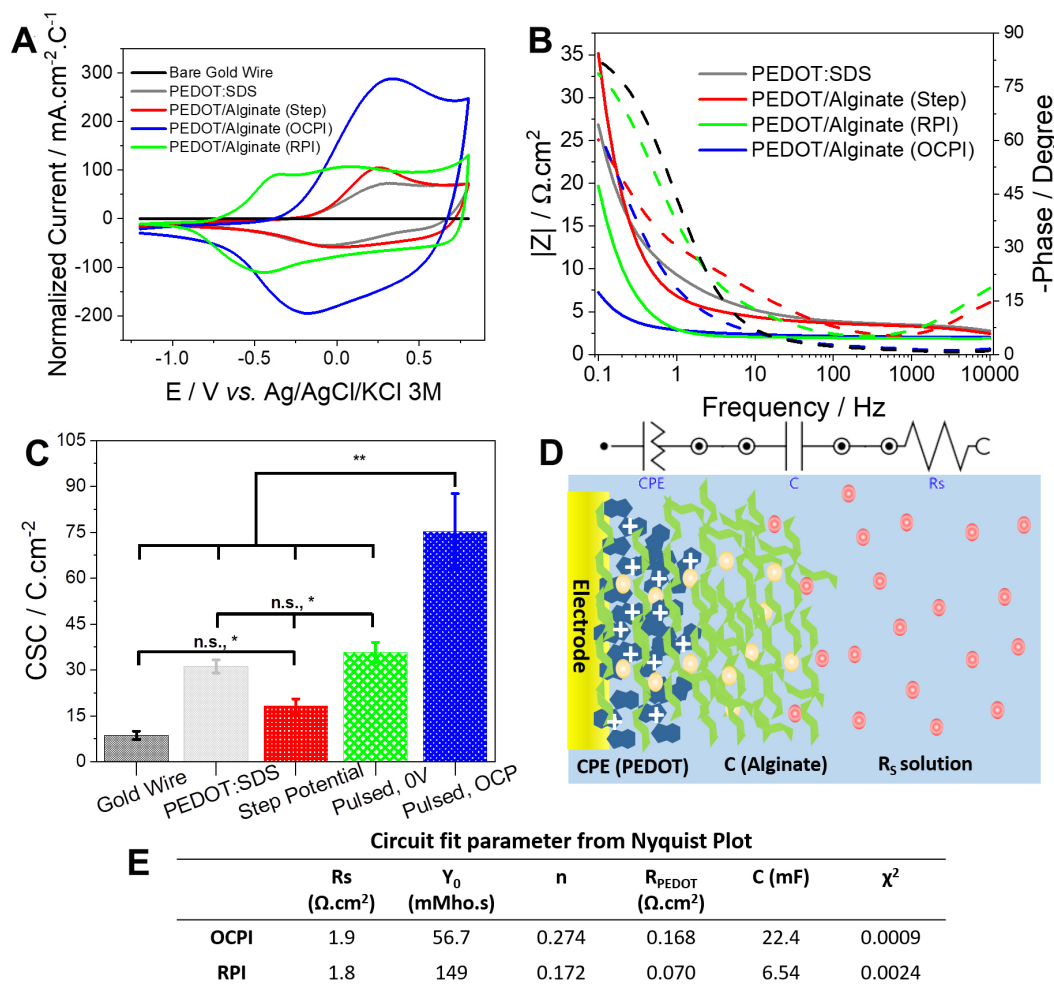


Figure 3. Electrochemistry of the PEDOT/alginate interface. (A) Cyclic voltammograms (normalised by area and $Q_{\text{electrodeposition}}$) for bare gold wire (black), PEDOT:SDS (control without alginate, grey) and PEDOT/alginate structures electrodeposited with step potential (red), pulsed RPI protocol (green) and OCPI protocol (blue) in PBS (pH = 7.4) as supporting electrolyte and scan rate of 50 mV s^{-1} . (B) Bode plots showing impedance modulus (left axis, continuous line) and phase angle (right axis, dashed line) for PEDOT:SDS (control without alginate, grey) and PEDOT/alginate hydrogel electrodeposited with step potential (red), RPI protocol (green) and OCPI protocol (blue). (C) Charge storage capacity (CSC) measured in PBS for bare gold wire (black), PEDOT:SDS (control without alginate, grey) and PEDOT/alginate hydrogel electrodeposited with step potential (red), RPI protocol (green) and OCPI protocol (blue). Experiment was performed in triplicate over different gold wire electrodes. Error bars indicate one standard deviation of the mean. Statistical significance is determined by one-way analysis of variance (ANOVA)/Tukey correction, n.s. is non-significant $P > 0.05$, $*P < 0.05$ and $**P < 0.001$. (D) Equivalent circuit (top) and schematic (bottom) of the proposed molecular distribution in the core-shell structure. In the equivalent circuit, R_s represents solution resistance, CPE represents a constant phase element representing the doped PEDOT core and C is the capacitance of the alginate hydrogel shell. CPE elements are used for inhomogeneous or imperfect capacitance, comprising the parameters Y_0 and n , where Y_0 is a pseudocapacitance constant and n is the deviation from ideal capacitor behaviour ($n = 1$ for a pure capacitor and $n = 0$ for a pure resistor). (E) Table with values for all circuit components extracted from fitting experimental impedance spectra. R_{PEDOT} represents the electronic resistance due to PEDOT (see methods section) obtained from CPE where $n < 0.3$. χ^2 statistically represents the approximation between theoretical and experimental data.

The charge storage capacity (CSC) for bare gold wire (black), PEDOT:SDS (without alginate, grey) and the core-shell structures electrodeposited with step potential (1000 s, red), RPI (60 pulses, green) and OCPI (120 pulses, blue) protocols is presented in [Figure 3C](#). The charge was calculated from cyclic voltammograms and current density (mA cm^{-2}) [[Supplementary Figure 10](#)]. The core-shell structures obtained with the OCPI protocol presented significantly higher CSC compared to others. Additionally, those obtained with the RPI protocol did not present significant differences with the PEDOT:SDS and

electrodeposition (at $P < 0.05$). It is worth mentioning that PEDOT cores obtained using the RPI method have neutral structure (benzoid, [Figure 1A](#)); hence, less charge is stored in the PEDOT layer initially. However, the first CV cycle causes oxidation and the conductivity, electroactivity and interconnectivity significantly improve.

The behaviour of core-shell structures was also investigated by fitting an equivalent circuit model to EIS measurements [[Supplementary Figure 11](#)]. [Figure 3D](#) shows our proposed equivalent circuit (top) and a schematic representation of the core-shell structures (bottom). Assuming the interface between PEDOT and the alginate hydrogel is electrically integrated, the PEDOT should correspond to a constant phase element (CPE) that is both electronically and ionically conductive and connected in series with a capacitance (C) representing the ionically conductive alginate hydrogel. The supporting electrolyte (PBS) is modelled by a resistance (R_s). [Figure 3E](#) shows a table containing the values of the components extracted by fitting EIS spectra. We note a relatively low value for the CPE exponent (n) for the PEDOT element (0.274 and 0.172 for OCPI and RPI protocols, respectively). It suggests that here PEDOT acts more as a resistor (electronically conductive) than a capacitor. Resistor values (R_{PEDOT}) of 0.168 and 0.070 $\Omega \text{ cm}^2$ for OCPI and RPI protocols were extracted, respectively (see methods section). The capacitance (C) was found to be 22.4 and 6.54 mF for OCPI and RPI protocols, respectively. These observations agree with our previous characterizations [[Figure 2](#)] where the interface produced using OCPI protocol is fully doped (i.e., loaded with charges), while the interface produced using RPI protocol is fully dedoped (i.e., neutral). In addition, the major contribution to the capacitance (C) should come from a thicker alginate layer. A strong influence of the initial doping state of PEDOT on the capacitance of the alginate compartment suggests good integration between the two materials.

The electrochemical properties of a number of PEDOT/alginate materials reported in the literature are presented in [Table 1](#). The current densities supported by the reported materials range from 5 $\mu\text{A cm}^{-2}$ to 1 mA cm^{-2} and PEDOT resistances range from 5 k Ω to 123 k Ω . The PEDOT/alginate structures reported here support significantly higher current density (60 mA cm^{-2} , [Supplementary Figure 10](#)) and lower R_{PEDOT} (0.168 $\Omega \text{ cm}^2$ for the OCPI protocol). As compared with composite or blending approaches, our work demonstrates enhanced electrical properties, likely due to improved integration between the PEDOT and alginate.

Loading and Release of a negatively charged small molecule. We used fluorescein (widely known as model negatively charged small molecule^[50-52]) to explore the potential of core-shell structures as encapsulation and delivery system. To encapsulate the target molecule in both the PEDOT (core) and alginate (shell) compartments in a single step, we added 1 mg mL^{-1} of fluorescein to the electrodeposition solution [[Figure 4](#)]. Our approach differs from previously reported work where the hydrogel is prepared first and then loaded either passively or by oxidizing the conducting polymer chain in the presence of the cargo molecule (and other ions as well)^[53-56]. [Figure 4A](#) and [B](#) show a schematic representation and a photograph of the structures loaded with fluorescein.

Our integrated interface consists of two distinct compartments: (1) the alginate shell capable of passively releasing the target molecule (top, green); and (2) the PEDOT core capable of electrically controlled release (bottom, blue). As the cargo molecule is negatively charged, the OCPI protocol was employed here to generate oxidized PEDOT (positively charged). The amount of loaded fluorescein can be inferred by fully releasing the cargo from both compartments. [Figure 4C](#) shows the concentration of fluorescein embedded in the alginate volume (i.e., excluding any fluorescein embedded in PEDOT core). This was obtained by completely dissolving the alginate layer with sodium citrate (50 mM). Interestingly, for the hybrid gel

Table 1. Comparison between CVs and PEDOT resistance for PEDOT/Alginate materials

Name	Method	Current density	R _{PEDOT} [§]	Reference
PEDOT/Alginate hydrogel	PEDOT:PSS in Alginate matrix	~8 $\mu\text{A cm}^{-2}$, 100 mM CaCl_2	62.9 k Ω	García-Torres, <i>et al.</i> ^[27]
PEDOT:PSS/Alginate	Microelectrode array, PEDOT:PSS mixed in Alginate matrix	-0.8 μA^* , PBS	5-30 k Ω [#]	Ghezzi, <i>et al.</i> ^[16]
Alginate-PCNT-PEDOT/PSS hydrogel	Microwire, PEDOT:PSS coated MWCNT in Alginate hydrogel	-1 mA cm^{-2} , 9% NaCl	123 k Ω	Wang, <i>et al.</i> ^[23]
PEDOT/hydrogel/BDNF-coated implants	Pt/Ir cochlear implant (microelectrode), electrodeposition of PEDOT:PSS	-3 μA^* , PBS	-	Chikar, <i>et al.</i> ^[24]
PEDOT ₇ Alg ₃	PEDOT/Alginate scaffolds	300 μA^* , not informed	-	Yang, <i>et al.</i> ^[25]
Hybrid PEDOT/Alginate hydrogel	Macroelectrode (centimeter size) electrodeposition, pulsed method	60 mA cm^{-2} , PBS	0.168 $\Omega \text{ cm}^2$ (2.1 Ω)	Present work

*Current density not reported, only current value; [§]Value reported for R_{CT} (charge transfer); [#]Value reported as total impedance at 1 kHz. CV: Cyclic voltammetry; PBS: phosphate saline buffer.

produced with 120 pulses, the concentration of encapsulated fluorescein is higher than the concentration in the bulk solution (1 mg mL⁻¹, red dotted line). This is likely due to the SDS micelles assisting in concentrating the target molecules. Initially, the concentration increases linearly with pulse number following the growth kinetics of the shell. Beyond 120 pulses, the concentration decreases, likely because of the change in growth kinetics previously discussed [Figure 2]. Figure 4D shows the fluorescein amount passively released (gel submerged in PBS for 24 h) from core-shell structures formed with different amounts of charge/pulse number. Within experimental error, we observe a constant amount of released fluorescein per total charge unit (Q_{ox}^{total}) (no significant difference $P > 0.005$). Figure 4E shows the temporal profile of fluorescein release from the shell compartment (green, left axis) and the evolution of the interface impedance (modulus, at 1 Hz). Although other effects cannot be ruled out, it appears that the decrease in impedance correlates with the release of fluorescein and can thus be used to monitor the process.

For studying electroactive release from the PEDOT core, the alginate layer was first dissolved in sodium citrate. Figure 4F shows the electroactive release of fluorescein under different electric potentials (within the aqueous electrochemical window) applied for 40 min in PBS media. The lower the electric potential applied, the higher the amount of fluorescein released. Additionally, it is worth mentioning that the amount of fluorescein stored in the PEDOT core compartment (and available for controlled release) is roughly 10 times lower than that in the alginate shell (passive release) compartment. Figure 4G shows the total amount of fluorescein electrically released as function of the charge supplied for core-shell structure formation (Q_{ox}^{total}). In contrast with the alginate shell component [Figure 4D], we obtained a linear increase in the amount of fluorescein encapsulated that follows order zero kinetics ($1.94 \pm 0.18 \mu\text{g C}^{-1}$, $r = 0.9823$). Although several approaches using electrodeposited conducting polymers as delivery systems exist, as far as we know, the correlation between electrodeposition charge and the amount of molecules encapsulated has not been reported before^[57,58]. Figure 4H demonstrates controlled release of fluorescein from the PEDOT compartment at different potentials. We have defined 40 min for each of the release experiments for didactical purpose, but the duration of electroactive release could potentially be extended for significantly longer. In the release-OFF condition, where +0.8 V was applied for the whole experiment, fluorescein is nearly fully retained in the PEDOT compartment. Under the passive release condition, where no external potential was applied, 6%wt of the total fluorescein load was released after 40 min. In the release-ON condition, -1.2 V was applied for the whole experiment, fully releasing the target molecule in approximately 15 min. The ON condition shows the maximum rate at which the target molecule can be delivered. For

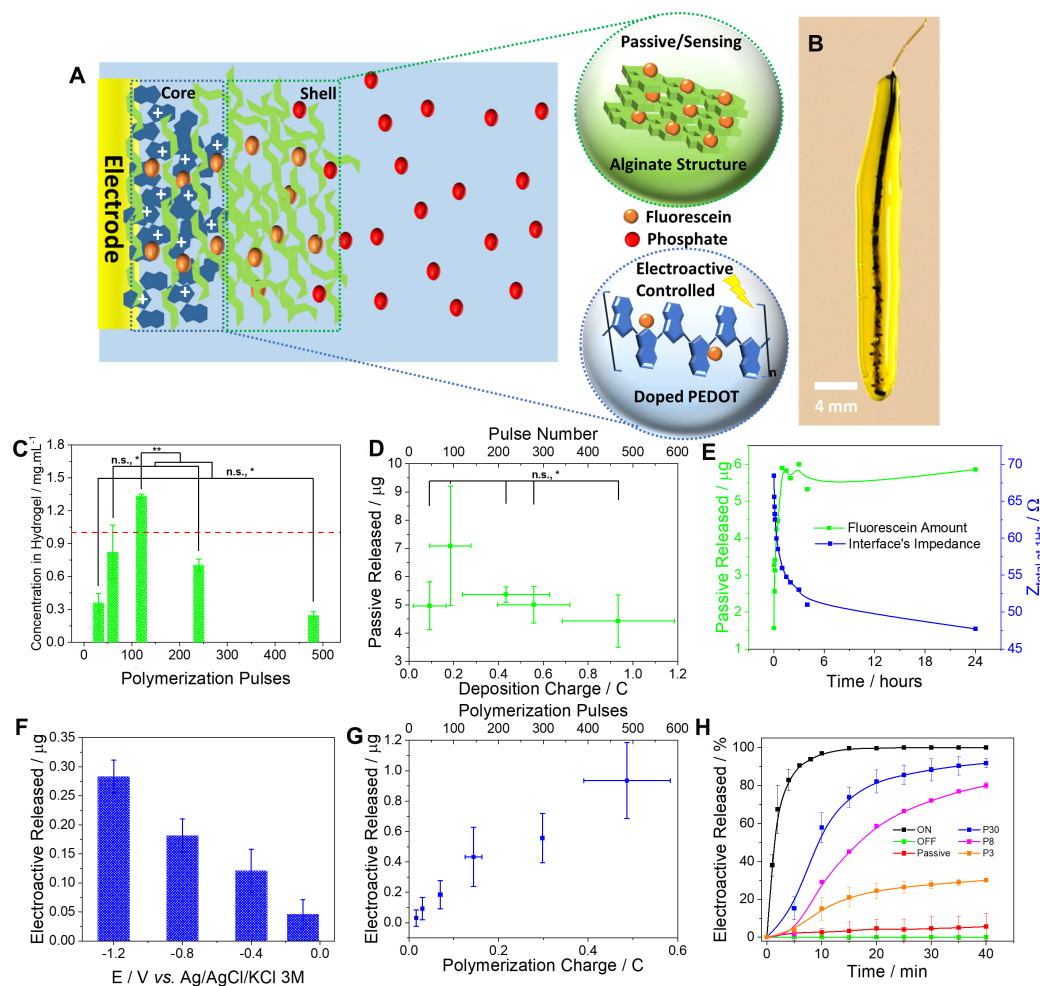


Figure 4. Passive/sensing release and electroactive controlled release of fluorescein. (A) Schematic representation of the core-shell structure. Shell compartment: passive release from the alginate layer. Core compartment: electroactive controlled release from PEDOT (quinoid structure, bottom). (B) Photograph of the core-shell structure loaded with fluorescein. (C) Concentration of fluorescein encapsulated in the volume of the alginate shell. The horizontal dashed line (red) indicates the fluorescein concentration in the polymerisation solution (1 mg mL⁻¹). (D) Relationship between the amount of fluorescein encapsulated in the shell and the polymerisation charge applied to form the core-shell structure. Statistical analyses for (C and D) were made in triplicate over three different gold wire electrodes. Statistical significance was determined using one-way analysis of variance (ANOVA)/Tukey correction, n.s. is non-significant ($P > 0.05$), $*P < 0.05$ and $**P < 0.001$. (E) Passive release of fluorescein quantified by fluorescence (green, left axis) and total impedance change of the interface (blue, right axis). (F) Amount of fluorescein actively released from the core at different electric potentials. Each release experiment lasts 40 min. (G) Relationship between the amount of fluorescein encapsulated in the core and the polymerisation charge applied for core-shell structure formation. (H) Electroactive release of fluorescein under controlled conditions: ON (black, -1.2 V), OFF (green, +0.8 V), passive (red, OCP), P30 (blue, pulse for 30 s at -1.2 V), P8 (purple, pulse for 8 s at -1.2 V) and P3 (orange, pulse for 3 s at -1.2 V). For the electrically controlled release, the programmed pulse is applied every 5 min.

tuning the release rate, we programmed a series of pulses consisting of either 30 (P30, blue), 8 (P8, purple) or 3 (P3, orange) seconds release-ON potential followed by holding at OCP. The pulsed protocol demonstrates that release rates can be tuned, which is critically important for sustainable release applications^[59,60].

CONCLUSIONS

In this work, we describe single-step electrosynthesis of conductive core-shell structures of PEDOT and alginate hydrogel. For this, we developed pulsed protocols to enhance the growth of the alginate

compartment. Charge considerations enable us to determine the amount of electrodeposited materials, and their growth kinetics. Electrochemical characterization revealed that the interface is highly electroactive, indicating good integration between the PEDOT and alginate compartments. We loaded the structures with a negatively charged model molecule for demonstration of passive release (and its monitoring) and controlled electroactive release from the alginate and PEDOT compartments, respectively. Our electro-assisted assembly and loading approach may contribute to the design of electrical hydrogel devices for applications in biointerfaces and soft electronics. For instance, in the context of implantable electrode arrays, the alginate shell compartment may enable burst release of a high dose of a drug (e.g., the anti-inflammatory drug dexamethasone), loaded vesicles or encapsulated cells, while the PEDOT core compartment can provide sustained long-term maintenance dosing.

DECLARATIONS

Authors' contributions

Conceived the idea: Da Silva AC, Minev IR

Planned and performed the experiments: Da Silva AC

Performed SEM analysis and fluorescence quantification: Paterson TE

Analysed results and wrote the manuscript: Da Silva AC, Paterson TE, Minev IR

Availability of data and materials

Not applicable.

Financial support and sponsorship

All authors acknowledge funding from ERC Starting Grant: IntegraBrain (804005). We acknowledge assistance from Christopher Hill, Department of Molecular Biology and Biotechnology for SEM-EDS and CPD analysis.

Conflicts of Interest

All authors declared that there are no conflicts of interest.

Ethical approval and consent to participate

Not applicable.

Consent for publication

Not applicable.

Copyright

© The Author(s) 2023.

REFERENCES

1. Tringides CM, Boulingre M, Khalil A, Lungjangwa T, Jaenisch R, Mooney DJ. Tunable conductive hydrogel scaffolds for neural cell differentiation. *Adv Healthc Mater* 2022:e2202221. DOI PubMed
2. Freudenberg U, Atallah P, Limasale YDP, Werner C. Charge-tuning of glycosaminoglycan-based hydrogels to program cytokine sequestration. *Faraday Discuss* 2019;219:244-51. DOI PubMed
3. Simpliciano C, Clark L, Asi B, et al. Cross-linked alginate film pore size determination using atomic force microscopy and validation using diffusivity determinations. *J Surf Eng Mater Adv Technol* 2013;03:1-12. DOI
4. Rastogi P, Kandasubramanian B. Review of alginate-based hydrogel bioprinting for application in tissue engineering. *Biofabrication* 2019;11:042001. DOI PubMed
5. Correa S, Grosskopf AK, Lopez Hernandez H, et al. Translational applications of hydrogels. *Chem Rev* 2021;121:11385-457. DOI
6. Paulsen BD, Fabiano S, Rivnay J. Mixed ionic-electronic transport in polymers. *Annu Rev Mater Res* 2021;51:73-99. DOI
7. Rong Q, Lei W, Liu M. Conductive hydrogels as smart materials for flexible electronic devices. *Chemistry* 2018;24:16930-43. DOI

[PubMed](#)

8. Distler T, Boccaccini AR. 3D printing of electrically conductive hydrogels for tissue engineering and biosensors - A review. *Acta Biomater* 2020;101:1-13. [DOI](#) [PubMed](#)
9. Shur M, Fallegger F, Pirondini E, et al. Soft printable electrode coating for neural interfaces. *ACS Appl Bio Mater* 2020;3:4388-97. [DOI](#)
10. Tondera C, Akbar TF, Thomas AK, et al. Highly conductive, stretchable, and cell-adhesive hydrogel by nanoclay doping. *Small* 2019;15:e1901406. [DOI](#) [PubMed](#)
11. Bhat MA, Rather RA, Shalla AH. PEDOT and PEDOT:PSS conducting polymeric hydrogels: a report on their emerging applications. *Synth Met* 2021;273:116709. [DOI](#)
12. Boehler C, Aqrave Z, Asplund M. Applications of PEDOT in bioelectronic medicine. *Bioelectron Med* 2019;2:89-99. [DOI](#)
13. Heo DN, Lee SJ, Timsina R, Qiu X, Castro NJ, Zhang LG. Development of 3D printable conductive hydrogel with crystallized PEDOT:PSS for neural tissue engineering. *Mater Sci Eng C* 2019;99:582-90. [DOI](#) [PubMed](#)
14. Fu F, Wang J, Yu J. Interpenetrating PAA-PEDOT conductive hydrogels for flexible skin sensors. *J Mater Chem C* 2021;9:11794-800. [DOI](#)
15. Lacour SP, Courtine G, Guck J. Materials and technologies for soft implantable neuroprostheses. *Nat Rev Mater* 2016;1:16063. [DOI](#)
16. Ferlauto L, D'Angelo AN, Vagni P, et al. Development and characterization of PEDOT:PSS/alginate soft microelectrodes for application in neuroprosthetics. *Front Neurosci* 2018;12:648. [DOI](#) [PubMed](#) [PMC](#)
17. Shi H, Liu C, Jiang Q, Xu J. Effective approaches to improve the electrical conductivity of PEDOT:PSS: a review. *Adv Electron Mater* 2015;1:1500017. [DOI](#)
18. Liu Y, Liu J, Chen S, et al. Soft and elastic hydrogel-based microelectronics for localized low-voltage neuromodulation. *Nat Biomed Eng* 2019;3:58-68. [DOI](#) [PubMed](#)
19. Lu B, Yuk H, Lin S, et al. Pure PEDOT:PSS hydrogels. *Nat Commun* 2019;10:1043. [DOI](#) [PubMed](#) [PMC](#)
20. Li G, Huang K, Deng J, et al. Highly conducting and stretchable double-network hydrogel for soft bioelectronics. *Adv Mater* 2022;34:e2200261. [DOI](#) [PubMed](#)
21. Li G. PEDOT:PSS-based intrinsically soft and stretchable bioelectronics. *Soft Sci* 2022;2:7. [DOI](#)
22. Cheng T, Zhang Y, Wang S, et al. Conductive hydrogel-based electrodes and electrolytes for stretchable and self-healable supercapacitors. *Adv Funct Mater* 2021;31:2101303. [DOI](#)
23. Wang K, Tian L, Wang T, et al. Electrodeposition of alginate with PEDOT/PSS coated MWCNTs to make an interpenetrating conducting hydrogel for neural interface. *Compos Interfaces* 2019;26:27-40. [DOI](#)
24. Chikar JA, Hendricks JL, Richardson-Burns SM, Raphael Y, Pflingst BE, Martin DC. The use of a dual PEDOT and RGD-functionalized alginate hydrogel coating to provide sustained drug delivery and improved cochlear implant function. *Biomaterials* 2012;33:1982-90. [DOI](#) [PubMed](#) [PMC](#)
25. Yang B, Yao F, Ye L, et al. A conductive PEDOT/alginate porous scaffold as a platform to modulate the biological behaviors of brown adipose-derived stem cells. *Biomater Sci* 2020;8:3173-85. [DOI](#) [PubMed](#)
26. Paradee N, Sirivat A. Electrically controlled release of benzoic acid from poly(3,4-ethylenedioxythiophene)/alginate matrix: effect of conductive poly(3,4-ethylenedioxythiophene) morphology. *J Phys Chem B* 2014;118:9263-71. [DOI](#) [PubMed](#)
27. Babeli I, Ruano G, Puiggali-jou A, Ginebra M, Alemán C, Garcia-torres J. Self-healable and eco-friendly hydrogels for flexible supercapacitors. *Adv Sustain Syst* 2021;5:2000273. [DOI](#)
28. Guo J, Yu Y, Wang H, Zhang H, Zhang X, Zhao Y. Conductive polymer hydrogel microfibers from multiflow microfluidics. *Small* 2019;15:e1805162. [DOI](#) [PubMed](#)
29. Madduma-bandarage USK, Madihally SV. Synthetic hydrogels: synthesis, novel trends, and applications. *J Appl Polym Sci* 2021;138:50376. [DOI](#)
30. Ji D, Park JM, Oh MS, et al. Superstrong, superstiff, and conductive alginate hydrogels. *Nat Commun* 2022;13:3019. [DOI](#) [PubMed](#) [PMC](#)
31. Yuk H, Zhang T, Lin S, Parada GA, Zhao X. Tough bonding of hydrogels to diverse non-porous surfaces. *Nat Mater* 2016;15:190-6. [DOI](#) [PubMed](#) [PMC](#)
32. Feig VR, Tran H, Lee M, et al. An Electrochemical gelation method for patterning conductive PEDOT:PSS hydrogels. *Adv Mater* 2019;31:e1902869. [DOI](#) [PubMed](#)
33. Inoue A, Yuk H, Lu B, Zhao X. Strong adhesion of wet conducting polymers on diverse substrates. *Sci Adv* 2020;6:eaay5394. [DOI](#) [PubMed](#) [PMC](#)
34. Yang J, Bai R, Chen B, Suo Z. Hydrogel adhesion: a supramolecular synergy of chemistry, topology, and mechanics. *Adv Funct Mater* 2020;30:1901693. [DOI](#)
35. Azmi S, Frackowiak E. Redox activity from the electrolyte and electrode in electrochemical capacitors. *Electrochem Commun* 2022;138:107289. [DOI](#)
36. Silva AC, Wang J, Minev IR. Electro-assisted printing of soft hydrogels via controlled electrochemical reactions. *Nat Commun* 2022;13:1353. [DOI](#) [PubMed](#) [PMC](#)
37. Silva AC, Akbar TF, Paterson TE, Werner C, Tondera C, Minev IR. Electrically controlled click-chemistry for assembly of bioactive hydrogels on diverse micro- and flexible electrodes. *Macromol Rapid Commun* 2022;43:e2200557. [DOI](#) [PubMed](#)
38. Fernandes R, Wu L, Chen T, et al. Electrochemically induced deposition of a polysaccharide hydrogel onto a patterned surface.

- Langmuir* 2003;19:4058-62. [DOI](#)
39. Cheng Y, Luo X, Betz J, et al. In situ quantitative visualization and characterization of chitosan electrodeposition with paired sidewall electrodes. *Soft Matter* 2010;6:3177. [DOI](#)
 40. Gray KM, Liba BD, Wang Y, et al. Electrodeposition of a biopolymeric hydrogel: potential for one-step protein electroaddressing. *Biomacromolecules* 2012;13:1181-9. [DOI](#) [PubMed](#)
 41. Cheng Y, Luo X, Betz J, Payne GF, Bentley WE, Rubloff GW. Mechanism of anodic electrodeposition of calcium alginate. *Soft Matter* 2011;7:5677. [DOI](#)
 42. Kim E, Xiong Y, Cheng Y, et al. Chitosan to connect biology to electronics: fabricating the bio-device interface and communicating across this interface. *Polymers* 2015;7:1-46. [DOI](#)
 43. Liu Y, Zhang B, Gray KM, et al. Electrodeposition of a weak polyelectrolyte hydrogel: remarkable effects of salt on kinetics, structure and properties. *Soft Matter* 2013;9:2703. [DOI](#)
 44. Li J, Kim E, Gray KM, et al. Mediated electrochemistry to mimic biology's oxidative assembly of functional matrices. *Adv Funct Mater* 2020;30:2001776. [DOI](#)
 45. Córdoba-torres P. Relationship between constant-phase element (CPE) parameters and physical properties of films with a distributed resistivity. *Electrochim Acta* 2017;225:592-604. [DOI](#)
 46. Hirschorn B, Orazem ME, Tribollet B, et al. Determination of effective capacitance and film thickness from constant-phase-element parameters. *Electrochim Acta* 2010;55:6218-27. [DOI](#)
 47. Sakmeche N, Aaron JJ, Fall M, et al. Anionic micelles; a new aqueous medium for electropolymerization of poly(3,4-ethylenedioxythiophene) films on Pt electrodes. *Chem Commun* 1996:2723. [DOI](#)
 48. Anastas P, Eghbali N. Green chemistry: principles and practice. *Chem Soc Rev* 2010;39:301-12. [DOI](#) [PubMed](#)
 49. Hutton LA, Vidotti M, Patel AN, Newton ME, Unwin PR, Macpherson JV. Electrodeposition of nickel hydroxide nanoparticles on boron-doped diamond electrodes for oxidative electrocatalysis. *J Phys Chem C* 2011;115:1649-58. [DOI](#)
 50. Kleber C, Lienkamp K, Rühle J, Asplund M. Electrochemically Controlled drug release from a conducting polymer hydrogel (PDMAAp/PEDOT) for local therapy and bioelectronics. *Adv Healthc Mater* 2019;8:e1801488. [DOI](#) [PubMed](#)
 51. Bazylevich A, Patsenker LD, Gellerman G. Exploiting fluorescein based drug conjugates for fluorescent monitoring in drug delivery. *Dye Pigment* 2017;139:460-72. [DOI](#)
 52. Jamwal HS, Chauhan GS. Designing silica-based hybrid polymers and their application in the loading and release of fluorescein as a model drug and diagnostic agent. *Adv Polym Technol* 2018;37:411-8. [DOI](#)
 53. Bagheri B, Zarrintaj P, Surwase SS, et al. Self-gelling electroactive hydrogels based on chitosan-aniline oligomers/agarose for neural tissue engineering with on-demand drug release. *Colloids Surf B Biointerfaces* 2019;184:110549. [DOI](#) [PubMed](#)
 54. Liang Y, Zhao X, Hu T, et al. Adhesive hemostatic conducting injectable composite hydrogels with sustained drug release and photothermal antibacterial activity to promote full-thickness skin regeneration during wound healing. *Small* 2019;15:e1900046. [DOI](#) [PubMed](#)
 55. Qu J, Liang Y, Shi M, Guo B, Gao Y, Yin Z. Biocompatible conductive hydrogels based on dextran and aniline trimer as electro-responsive drug delivery system for localized drug release. *Int J Biol Macromol* 2019;140:255-64. [DOI](#) [PubMed](#)
 56. Qu J, Zhao X, Ma PX, Guo B. Injectable antibacterial conductive hydrogels with dual response to an electric field and pH for localized "smart" drug release. *Acta Biomater* 2018;72:55-69. [DOI](#) [PubMed](#)
 57. Bansal M, Dravid A, Aqrave Z, Montgomery J, Wu Z, Svirskis D. Conducting polymer hydrogels for electrically responsive drug delivery. *J Control Release* 2020;328:192-209. [DOI](#) [PubMed](#)
 58. Park Y, Jung J, Chang M. Research progress on conducting polymer-based biomedical applications. *Appl Sci* 2019;9:1070. [DOI](#)
 59. Cao Y, Samy KE, Bernards DA, Desai TA. Recent advances in intraocular sustained-release drug delivery devices. *Drug Discov Today* 2019;24:1694-700. [DOI](#) [PubMed](#) [PMC](#)
 60. Lowinger MB, Barrett SE, Zhang F, Williams RO 3rd. Sustained release drug delivery applications of polyurethanes. *Pharmaceutics* 2018;10:55. [DOI](#) [PubMed](#) [PMC](#)